communications sustainability

A Nature Portfolio journal

Article

https://doi.org/10.1038/s44458-026-00157-0

Rooftop solar supports carbon-neutral transition in Hong Kong's building sector

Check for updates

Lai Yiu Tong [1], Zhiwei Li [2,3] ✉, Cheolhee Yoo [4], Siqi Jia [5], Rui Zhu [6,7] & Jungho Im [3,8,9] ✉

Rooftop solar systems are pivotal for carbon neutrality and urban sustainability, yet accurate assessment of rooftop solar energy potential remains constrained by coarse representation of complex building forms, incomplete characterization of cloud variability, and limited integration of technical, economic, and policy factors. Here we show that a machine learning framework integrating high-frequency satellite and ground observations can estimate rooftop solar energy potential at 0.5-meter resolution for 338,550 buildings in Hong Kong. Despite substantial reductions associated with cloud cover and temperature, total citywide potential reaches 3.77 terawatt-hours per year. This resource could avoid 24.9 billion kilograms of carbon dioxide emissions over its lifetime and enable 18.9% of commercial buildings with energy storage to achieve local decarbonization targets. Supported by local feed-in tariffs, average financial payback periods range from 3.49 to 6.42 years, with more than 90% of buildings meeting household affordability thresholds. These findings provide actionable guidance for solar deployment, investment decisions, and urban energy planning in dense, cloud-prone cities worldwide.

Rooftop solar photovoltaics (PV) offer a practical lever for urban decarbonization by displacing fossil fuel-based electricity generation[1–3]. Beyond carbon mitigation, co-benefits include improved air quality[4], lower energy bills[5], reduced macro-economic pressure on the energy transition[6], and alleviated grid demand[7]. By shading building envelopes, rooftop PV can also limit heat gain through concrete roofs, enhance indoor thermal comfort, and curb cooling energy demand[8]. Yet, in Hong Kong, one of the world's most densely-built cities, solar PV contributes only 0.37% of the local power generation mix[9].

In high-density cities, solar adoption is limited not only by roof geometry[10–12], but also atmospheric condition[13–16], techno-economic feasibility[17–20], and policy structure[21–23]. Accurately quantifying these interlinked constraints through a hierarchical assessment framework—sequentially spanning from physical, geographical, technical, and economic potentials to carbon mitigation benefits—is essential for realistic, credible decarbonization planning[24].

Physical potential represents the theoretical maximum solar irradiance on rooftops under all-sky conditions. Three critical uncertainties persist: (1) cloud attenuation—many assessments assume clear-sky conditions or simplify cloud effects[10,22]. A few maps incorporate annual cloud probability[25], but lack long-term validation of diurnal cloud dynamics[26]. (2) Model choice and interpretability—empirical relations such as Ångström–Prescott (A–P) equation[27,28] links the sunshine duration to global solar radiation (GSR) linearly[29], but exhibit variable skill across altitudes and seasons[30]; machine learning can improve accuracy and adaptability[31], albeit with interpretability challenges. (3) Temporal coverage—polar-orbiting satellites (MODIS, Sentinel-2, Landsat) are limited by discrete overpass times, preventing full capture of diurnal cloud variability[32]. Ground-mounted weather stations are subject to interruptions in measurements due to maintenance, calibration, sensor soiling, and instrument malfunctions. They often lack spatial coverage, leaving irradiance estimates uncertain for rooftops distant from stations. The integration of ground-based and high-frequency satellite observations offers a valuable pathway to reduce temporal uncertainty[33].

Geographical potential integrates building morphology, including roof geometry (slope, orientation, size), shading, and roof obstacles. Existing assessments at multiple scales remain coarse in km-level resolution or assume flat roofs, omitting detailed shading[1,4,22]. High-resolution annual

[1]Department of Land Surveying and Geospatial Science, The Hong Kong Polytechnic University, Hong Kong, China. [2]School of Resource and Environmental Sciences, Wuhan University, Wuhan, China. [3]Department of Civil, Urban, Earth, and Environmental Engineering, Ulsan National Institute of Science and Technology (UNIST), Ulsan, South Korea. [4]Smart City Convergence Major, Pusan National University, Busan, South Korea. [5]Department of Architecture, Faculty of Architecture, The University of Hong Kong, Hong Kong, China. [6]State Key Laboratory of Climate System Prediction and Risk Management, Nanjing Normal University, Nanjing, China. [7]Key Laboratory of Virtual Geographic Environment (Nanjing Normal University), Ministry of Education, Nanjing, China. [8]Graduate School of Artificial Intelligence, UNIST, Ulsan, South Korea. [9]Graduate School of Carbon Neutrality, UNIST, Ulsan, South Korea. ✉e-mail: lizw@whu.edu.cn; ersgis@unist.ac.kr

irradiance maps (1 m) exist[11,34], but typically simplify the cloud effect and lack territory-wide coverage. 3D building models—extruded from 2.5D building footprint with height attribute—facilitates inter-building shading simulation[10], yet near-field shading (roof obstacles) and far-field non-building shading (vegetation, mountainous terrain) remain uncertain[24]. Finer-resolution mapping is essential for enhancing the granularity of rooftop solar energy potential (SEP) assessments.

Technical potential transforms irradiance estimates into electrical output, further considering both PV module electrical efficiency and overall system performance ratio. Prior studies typically assume static, time-independent electrical efficiencies under standard test conditions[3,4,29,34], while higher operating temperatures reduce the conversion efficiencies[35]. The spatiotemporal variability in how ambient temperature affects PV module conversion efficiency remains underexplored. Temporally resolved analysis that integrates weather parameters such as ambient temperature with module performance is essential to inform climate-adaptive rooftop strategies.

Economic potential determines the achievable technical potential and is governed by financial viability, profitability, and affordability. The levelized cost of energy (LCOE) and net present value (NPV) offer standardized metrics for evaluating cost competitiveness across power generation sources and estimating profitability, respectively[4,36]. Yet, existing estimates of LCOE and NPV typically rely on country-level average costs and idealized technical potentials that assume cloud-free, shadow-free, and full rooftop utilization. Financial viability can be evaluated by pairing financial payback periods with households' affordability threshold. However, previous case studies have reported highly variable financial payback periods (9.6–72.5 years)[17,18,20], owing to small building samples and inconsistent revenue assumptions. A territory-wide, building-level assessment on economic potential is needed for context-specific urban energy transitions.

Carbon accounting shows similar gaps. Many studies focus on operational-phase carbon benefits while omitting full lifecycle emissions, including manufacturing, maintenance, transportation, decommissioning, and recycling[22,37,38], potentially overstating the net carbon benefits with shorter carbon paybacks. A full lifecycle balance at building scale is needed for robust environmental planning and impact assessment.

We address four major research gaps by delivering: an interpretable machine learning framework that integrates building morphologies with full diurnal cloud dynamics; high-resolution, territory-wide solar irradiance maps with long-term validation; a building-level, scenario-based economic analysis; and complete lifecycle carbon assessment for rooftop solar PV (Supplementary Fig. 1).

Here, we fuse multi-source remote sensing and ground observations to estimate SEP at 0.5 m resolution for 338,550 rooftops across Hong Kong over the period of 2016–2024. We (1) quantify cloud-induced attenuation on rooftop SEP; (2) present a high-resolution, citywide solar irradiation map for PV siting; (3) identify buildings and districts with the strongest financial and carbon gains; (4) assess financial feasibility, lifecycle carbon balance, and potential contributions to the *Climate Action Plan 2050*[39]. The proposed framework can be transferred to other high-density and cloud-prone cities worldwide, supporting urban sustainability and the global pursuit of carbon neutrality.

Results

Spatiotemporal patterns of rooftop SEP

Cloud cover strongly reshapes GSR. We computed annual GSR under clear-sky conditions using a hemispherical viewshed algorithm[40] and predicted the all-sky GSR with a machine learning model[41,42]. On average, all-sky GSR is ~50% lower than clear-sky values. Attenuation peaks in June–August (56.3%) and is weakest in December–February (34.2%), consistent with thicker and more frequent summer cloud fields. Rolling-window analysis (20-day) indicates a shift from a single-peak to a quadri-modal seasonal pattern under clouds, with a marked trough between day-of-year 206–280 that coincides with peak tropical-cyclone activity (Supplementary Fig. 2). Cloud variability thus governs both the magnitude and seasonality of rooftop GSR.

Multi-scale spatial analysis of rooftop SEP. Pixel-scale mapping reveals clear spatial structure across Hong Kong (Fig. 1). Lower GSR clusters along north-facing slopes framing Victoria Harbour and Tolo Channel, where complex relief and tall neighboring structures intensify shading. Higher values appear over old urban fabric (such as Sham Shui Po, Cheung Sha Wan, and Lai Chi Kok), village-type settlements (such as Yuen Long and Kam Sheung Road), and Hong Kong International Airport in Chek Lap Kok. Because electrical output depends on electrical efficiency, performance ratio, deployable roof area and solar irradiance incident on PV modules rather than solar irradiance alone, we convert GSR to rooftop SEP using Eq. (12).

At building resolution, large and unobstructed roofs (Fig. 2, red) emerge as candidates for high-capacity systems. Hong Kong International Airport (Chek Lap Kok)'s roofs are especially suitable for large-scale deployment with grid-connected storage to buffer Tung Chung peak demand. When overlaid with land use and land cover (LULC) data, urban residential buildings contribute ~34% of citywide annual SEP, followed by rural settlement (18%), industrial (16%) and institutional (12%); transport, commercial, and other land uses comprise around 19% (Supplementary Fig. 3 and Supplementary Table 1).

District-scale contrasts are pronounced (Fig. 3). Yuen Long yields the largest absolute SEP (0.718 TWh, 19.1% of the citywide total), whereas Wong Tai Sin contributes the lowest of 0.081 TWh (2.14%). Normalized by district roof area, Islands District leads (67.0 GWh/km²), followed closely by Yuen Long (62.4 GWh/km²) and North District (60.9 GWh/km²). Eastern is lowest (53.9 GWh/km²), with Wan Chai (54.2 GWh/km²) and Central and Western (54.6 GWh/km²) slightly higher (Supplementary Table 2).

After incorporating the temperature-dependent efficiency into technical potential modeling, we find that: first, the annual SEP estimates decrease from 3.85 to 3.77 TWh, due to reduced electrical efficiency when PV modules operate above standard testing temperature. Second, densely built urban environment and the airport experience more significant loss in annual SEP (Supplementary Fig. 4). Third, the total SEP loss is 96% higher in the warmer period (June–September) than in the colder period (December–February) (Supplementary Fig. 5).

Energy, economic, and carbon implications

Energy-saving and life-cycle carbon balance. Full utilization of deployable roof areas yields 3.77 TWh yr^{-1}, covering 4.98% of end-use energy and 8.28% of electricity consumption[9]. Avoided primary energy is equivalent to 369 thousand tonnes of coal, 274 thousand tonnes of natural gas, and 0.0502 tonnes of nuclear fuel annually, given the stated conversion factors.

Lifecycle accounting shows total carbon reduction of 36.7 billion kg-CO_2 versus lifecycle carbon emissions of 11.9 billion kg-CO_2, dominated by manufacturing (8.12), followed by decommissioning (2.403), transportation (0.572) and maintenance (0.812) (Fig. 4d). Net reduction is 24.9 billion kg-CO_2, with mean carbon payback of 8.18 years, ranging from 5.34 to 10.5 years. All buildings could potentially achieve carbon payback within the typical PV lifetime of 25 years[43] (Figs. 4c and 5e). This demonstrates significant potential for carbon mitigation across most building roofs.

Localizing PV manufacturing and end-of-life processing in Hong Kong could reduce lifecycle carbon emissions by 35.8% (from 11.9 to 7.87 billion kg-CO_2) primarily by shortening transport distances and replacing high-carbon grid electricity used in manufacturing and recycling with Hong Kong's relatively lower-carbon mix.

Economic feasibility at building scale. Rooftop solar PV systems across Hong Kong's 338,550 buildings demonstrate strong economic viability and profitability under current local FiT scheme, while remaining sensitive to policy support and upfront cost.

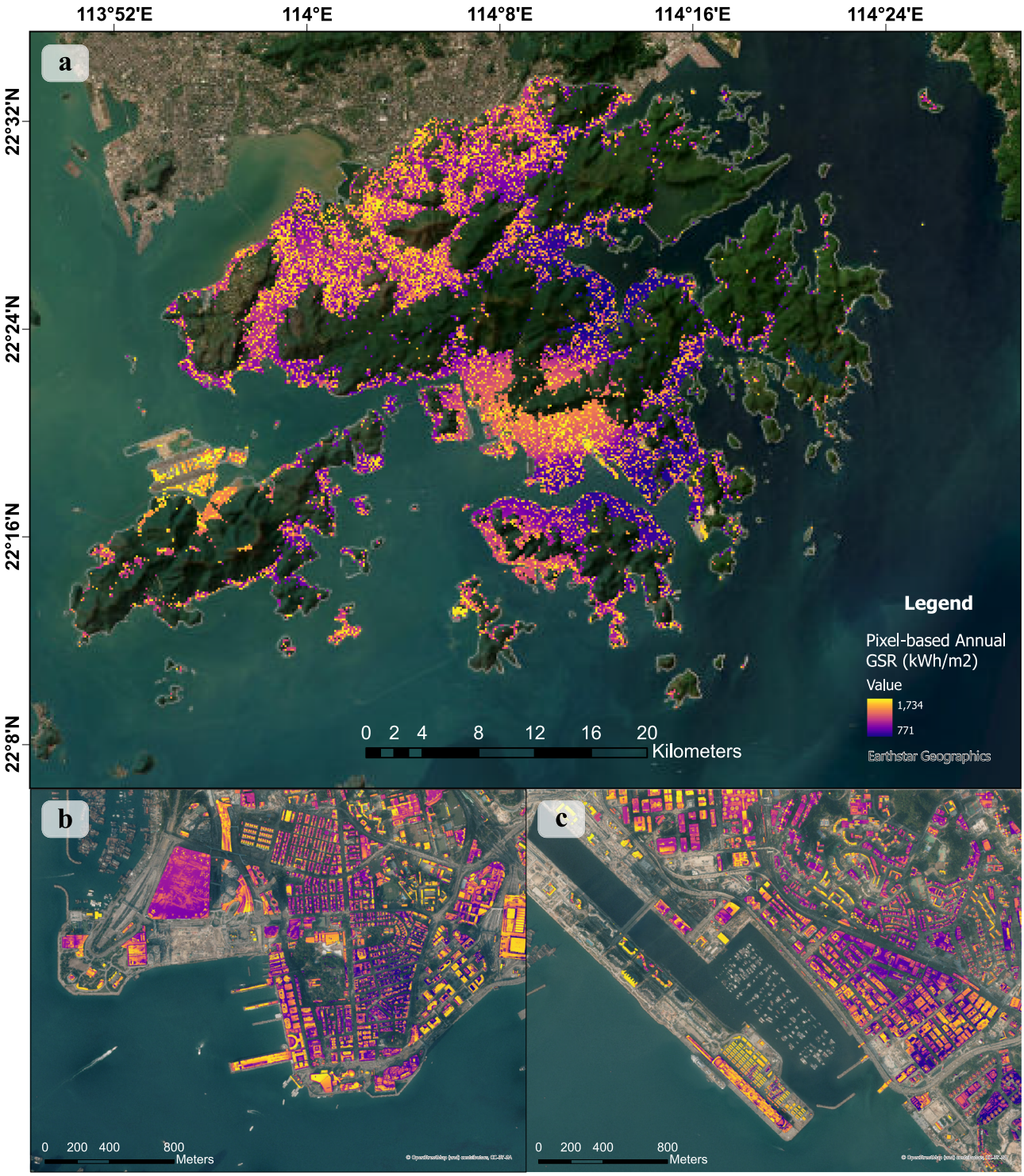


Fig. 1 | High-resolution (0.5 m) mapping of pixel-scale mean annual GSR for building roofs in Hong Kong under all-sky conditions (2016–2024). a Entire Hong Kong; **b** Tsim Sha Tsui; **c** Kai Tak and Kowloon Bay. This high-resolution (0.5 m) mapping product enables users to identify optimal rooftop areas for solar PV deployment. Bright yellow and dark indigo colors represent high and low GSR, respectively, under all-sky conditions and various building morphologies.

Under the FiT scheme[44], 100% of buildings could achieve LCOE below feed-in tariff rate in both the higher- and lower-capex scenarios (mean LCOE: 1.683 HKD/kWh and 1.018 HKD/kWh, respectively), illustrating that they are economically viable. For profitability, all buildings could yield positive NPV even under high-capex scenario (Mean: HKD 242,000), spanning from HK$1,150 to HK$ 87,400,000 (USD 147–USD 11,100,000), supported by the first-year mean revenue of HKD 36,500 (US$ 4650). For affordability, financial payback periods are highly attractive under lower-capex scenario (mean: 3.49 years; range: 2.66–7.02 years), with 100% of buildings repay within the typical 10-year household preference[19] and 25-year PV system lifespan[43] (Fig. 5a). Even under higher-capex scenario, financial paybacks remain favourable for the households (mean: 6.42 years; 4.74–14.99 years), with 99.6% achieving financial payback within 10 years and all within 25 years (Supplementary Table 3) (Fig. 5b).

In the absence of FiT support, net metering at the mean grid retail price (HK$ 1.5195/kWh) serves as the primary revenue source. While 100% of

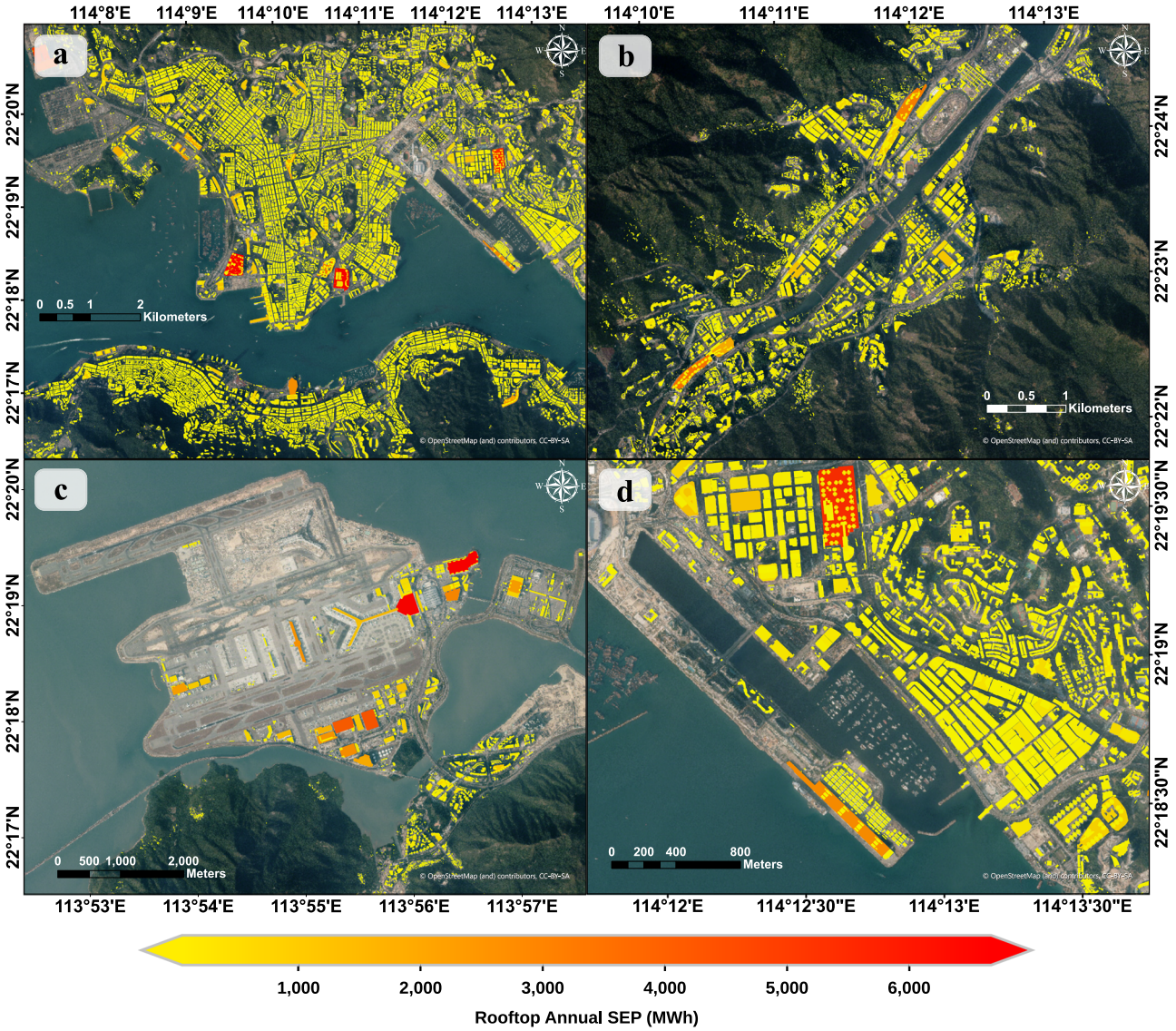


Fig. 2 | Mean annual rooftop SEP at the building level in Hong Kong (2016–2024). a Both sides of Victoria Harbor; **b** Sha Tin; **c** Hong Kong International Airport in Chek Lap Kok and Tung Chung; **d** Kai Tak and Kowloon Bay. This map can be used to identify building roofs with relatively higher potential for high-voltage solar PV deployment.

buildings could achieve grid parity (LCOE < grid retail price) and positive NPV under lower-capex scenario, only 0.75% do so under higher capex. Mean financial payback periods extend substantially to 11.58 years (range: 8.43–18.15 years) under lower capex (Fig. 5c), with only 1.06% of buildings meeting the 10-year household preference[19], and to 31.49 years (range: 19.31–51.70 years) at higher capex (Fig. 5d), without any building repay within the 10-year household preference[19] (Supplementary Table 3).

Potential contribution to the decarbonization targets in Hong Kong. Linking the Electrical and Mechanical Services Department (EMSD) building-level annual electricity use with rooftop SEP for 2,695 commercial buildings shows that 18.9% could potentially reduce their annual electricity demand drawn from the grid by ≥30% with full rooftop PV deployment, thereby increasing self-sufficiency; 6.90% could potentially meet or exceed their annual electricity demand, providing surplus to the grid via storage (Fig. 6b, c). Figure 6a highlights high-impact commercial buildings for the "Energy-saving and Green Building" target in Hong Kong's Climate Action Plan 2050[39].

Discussion

This study provides an integrated, analytical framework for rooftop SEP by overcoming critical challenges in data granularity, cloud modeling, techno-economic integration, and policy relevance. On data granularity, we employ high-resolution (0.5 m) LiDAR-derived DSMs to capture both near- and far-field shading from buildings, non-building objects like trees, terrain, and in-situ rooftop obstacles with greater fidelity than previous efforts[1,4,22,32]. On cloud modeling, we integrate ground-based all-sky GSR observations with high-frequency geostationary satellite cloud data to achieve full diurnal coverage of cloud dynamics, addressing the temporal gap on cloud uncertainty in prior work[10,11,22,25,26,31,34]. In techno-economic integration, we move beyond static PV module efficiency assumptions from existing studies[3,4,29,34] by accounting for dynamic thermal stress on module performance, thereby avoiding overestimation of technical potential. We also extend the research scope from technical potential[25,29,31] to broader context with building-level economic viability and lifecycle net carbon benefits for policy evaluation.

For policy relevance, our findings align with the three pillars of Hong Kong's Climate Action Plan 2050[39]. **Carbon Neutrality:** full rooftop deployment with energy storage integration could potentially contribute to abating 24.9 billion kg-CO_2, or around 42.0% of the remaining reduction needed from 2005 levels[45]. **Net-Zero Electricity Generation:** rooftop PV could potentially contribute to raising renewable shares from 2.57[9] to 10.2%, surpassing the 2035 target and potentially contribute to over half of the 2050 target[39]. **Energy-Saving and Green Building:** 18.9% of commercial

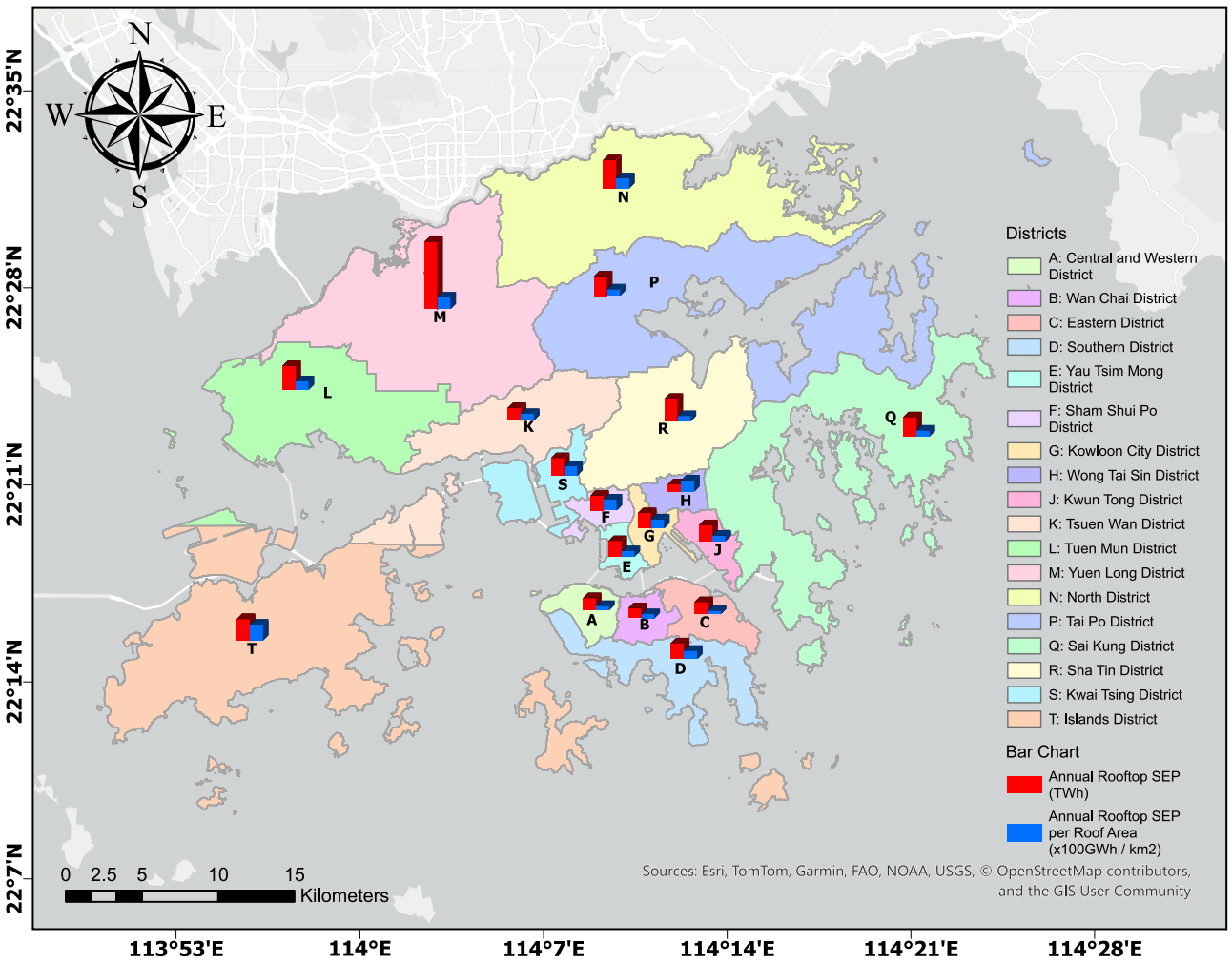


Fig. 3 | Mean annual rooftop SEP by district in Hong Kong (2016–2024). Red bars represent the total annual rooftop SEP for each district; blue bars represent the annual rooftop SEP per unit roof area, with values below 50 GWh/km^2 set to this minimum to enhance contrast among districts.

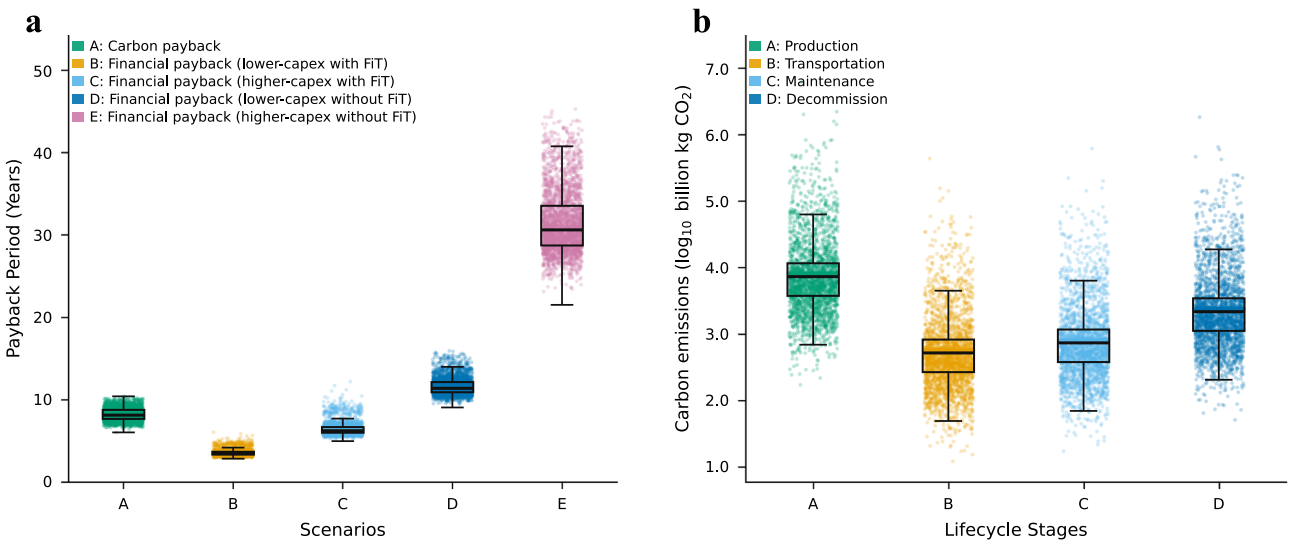


Fig. 4 | Building-level financial and carbon metrics for rooftop solar PVs in Hong Kong. a Carbon payback and financial payback periods under four capex-policy scenarios; **b** Building-level carbon emission breakdown of rooftop solar PV across the four lifecycle stages.

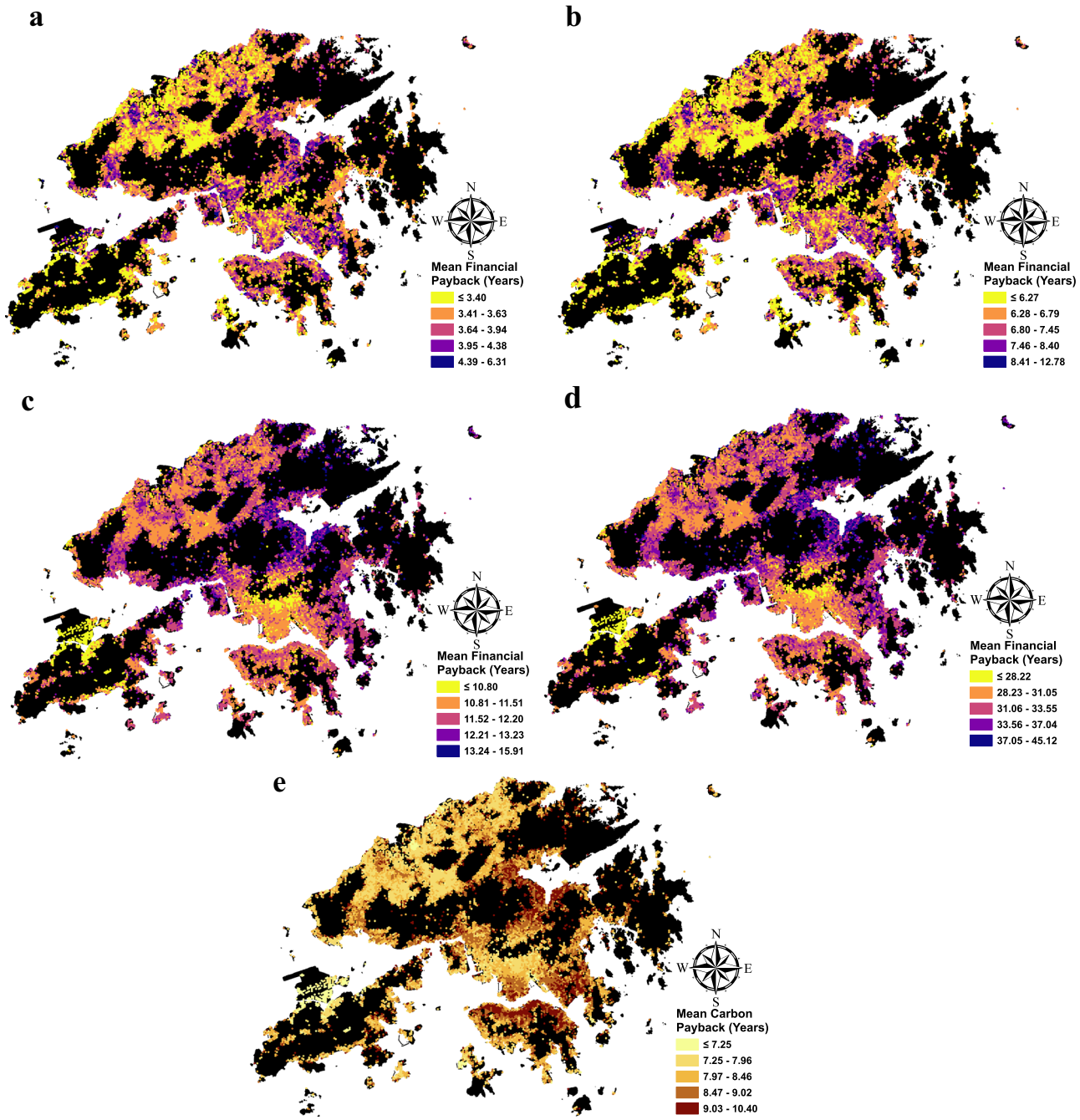


Fig. 5 | Building-level mean payback period for rooftop solar PV deployment in Hong Kong, where Jenks' natural break was adopted for data division. a mean financial payback at a lower capex of HK$30,000/kW with FiT subsidies; **b** mean financial payback at a higher capex of HK$50,000/kW with FiT subsidies; **c** mean financial payback at a lower capex of HK$30,000/kW without FiT subsidies; **d** mean financial payback at a higher capex of HK$50,000/kW without FiT subsidies; **e** mean carbon payback. For (**a–d**), bright yellow color indicates shorter mean financial payback periods, while dark indigo color indicates longer mean financial payback periods. For (**e**), yellow color indicates shorter mean carbon payback periods, while brown color indicates longer mean carbon payback periods.

buildings could potentially cut electricity drawn from the grid by >30% with storage-enabled self-consumption. Rooftops alone are not sufficient; complementary contributions from facades, open-area PV, and other renewables will be required to close the gap for carbon neutrality by 2050.

Despite these advances, several limitations should be acknowledged. First, our model training and validation currently rely on a limited number of ground stations due to data scarcity. Future work should expand observational networks through partnerships with NGOs, research institutes, governmental departments. Second, aerosol effect was omitted in this study, as cloud exerts a stronger influence on surface irradiance[14,46]; however, emerging evidence indicates that aerosol pollution from coal-fire plants[47] and extreme dust events[48] can substantially suppress PV output and thus should be incorporated in subsequent models. Third, although our cloud modeling provides full diurnal coverage, it falls short in capturing small cloud fragments due to coarse resolution. Advanced multi-source data fusion techniques could be explored to help address this challenge by better balancing spatial resolution, temporal coverage, and detail in cloud modeling. Fourth, our financial viability analyses and carbon benefit estimates assume full rooftop deployment, energy storage integration, and perfect building energy demand matching. Coupling our framework with urban building energy models[49] enables hourly mismatch analysis, supporting decision-making on energy storage capacity sizing, and refined economic

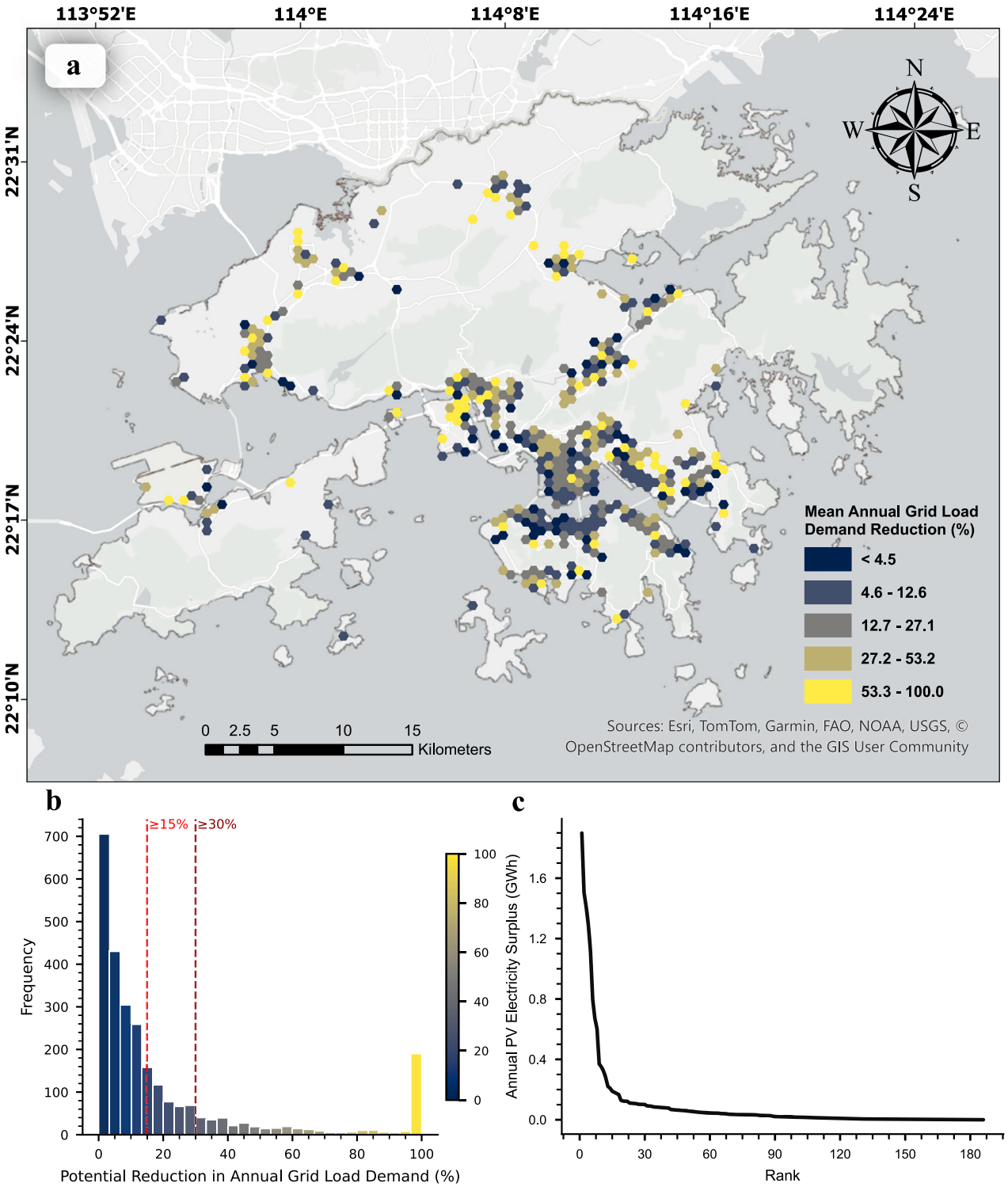


Fig. 6 | Potential contribution of rooftop solar PV deployment across 2,695 commercial buildings to the "Energy-saving and Green Buildings" decarbonization target in Hong Kong's Climate Action Plan 2050. a Spatial distribution of commercial buildings in Hong Kong, categorized by the mean annual grid load demand reduction with full deployment of rooftop solar PVs; **b** Frequency distribution of potential reduction in building-level annual grid load demand across all commercial buildings; **c** Ranking of annual PV electricity surplus across the commercial buildings that could potentially contribute to full electricity self-sufficiency.

viability and carbon benefit assessment, thereby informing green finance policy design for stable, long-run grid integration. Fifth, rooftop services are not explicitly masked due to data scarcity. While we consider statutory fire-safety setbacks, equating the building footprint to fully usable roof area may yield an overestimation of deployable PV. Integrating emerging cm-level LiDAR and drone survey data with object-based deep learning segmentation offers a promising avenue to refine deployable area estimates, and thus improve payback and carbon metrics. Sixth, while the economic framework

in this study includes the capex, opex with temporal change (e.g., discount rate and degradation rate on PV output), end-of-life cost is omitted. Future work shall perform full life-cycle cost analysis for robust economic feasibility assessment.

Even so, our study yields important insights for researchers and policy planners. First, cloud dynamics halve rooftop irradiance on annual average and restructure its seasonality, with the largest deficits in summer seasons. Our estimate (3.77 TWh) is approximately 37% lower than that of 5.98 TWh reported by ref. 38, who neglected cloud effects. Ignoring clouds inflates net carbon benefits and understates payback time estimates, with biases that are particularly acute in subtropical, cloud-prone climates. Second, our estimate is approximately 42% higher than the 2.66 TWh reported by ref. 25, who also explicitly accounted for cloud attenuation. This discrepancy arises potentially from a larger building stock, reduction in unauthorized rooftop structures, finer spatial resolution, and different assumptions on usable roof area and cloud modeling. These differences underscore the sensitivity of rooftop SEP estimates to spatial resolution, cloud dynamics, building morphology data, and modeling assumptions. Third, lifecycle results indicate that emissions from PV manufacturing, logistics, and end-of-life offset approximately one-third of operational benefits, which are larger than some earlier estimates[50,51]—owing to fossil fuel-intensive manufacturing and long-haul PV transport, and absence of local PV manufacturing, decommissioning, and recycling centres in Hong Kong. Decarbonizing PV supply chains and localized end-of-life handling could materially raise net benefits. Fourth, grid parity and economic viability could be potentially achievable across all buildings in Hong Kong under lower-capex scenarios (HK $30,000/kW) even without subsidies, consistent with national-scale findings from ref. 36, but become economically unviable for nearly all buildings under higher-capex scenarios (HK$50,000/kW), highlighting the significance of cost optimization in achieving grid parity. Coordinated bulk procurement[23], leveraging economies of scale and stronger supplier negotiations, represents a scalable pathway to capex reduction and accelerated deployment.

For policy implications, adoption hurdles persist under the prevailing policy structure. First, financial payback periods under the higher-capex scenario (range: 4.74–14.99 years) for 85.9% of buildings exceeds the remaining validity of the current FiT scheme (around 7 years), set to expire in 2033[44]. Extending or enhancing incentives, including FiT duration and rates, tax credits, carbon price or interest-free loans, may unlock high-potential sites. Future studies should analyze the potentials of transitioning towards net-metering or net-billing arrangement without subsidies to balance government fiscal burden and household affordability[24]. Second, cloud-driven power fluctuations pose a challenge to conventional battery longevity via ramp-rate stress[52]; technical solutions such as ramp-rate control[53], power-to-hydrogen approach[54] may improve storage flexibility. Policies for hydrogen storage transition could be further explored in future work. Third, deployable rooftop areas are constrained by structural capacity[55,56], available spaces on rooftops[18,19], and statutory fire-safety setbacks[57]. Mapping those undeployable roof areas digitally represents a crucial step to precisely identify suitable sites for PV siting.

In conclusion, our building-level maps provide actionable granularity: investors can target short-financial-payback roofs, and planners can prioritize districts that deliver the largest carbon and energy returns. By pairing this framework with decarbonized PV supply chains and complementary renewables, dense cities can accelerate progress toward resilient, net-zero power systems, supporting the United Nations' Sustainable Development Goal 13 (Climate Action). This research also highlights the inevitable role of government incentives in advancing Sustainable Development Goal 7 (Affordable and Clean Energy), by relieving financial burdens on rooftop solar PV deployment. Beyond the Hong Kong case, the integrated framework is highly transferable to other cloud-prone, high-density cities. It provides a unified framework for technical potential assessment, techno-economic analyses, and carbon accounting. However, successful scaling requires calibrating specific model inputs to the local context. These localized variables include meteorological data (cloud, ground-based temperature, and GSR data) and building morphological data (building footprints, DSM). Furthermore, economic potential relies on region-specific financial parameters (Capex, Opex, and discount rates), while carbon accounting depends on local emissions factors and lifecycle energy demands.

Methods

The methods encompass three major parts. The first part focuses on GSR modeling and validation. This part involves developing clear-sky GSR model, integrated with ground-based observation datasets using the A–P regression algorithm, or combined with both ground-based and satellite cloud mask datasets through a machine learning model. The optimal model is selected based on accuracy assessments. The second part focuses on rooftop SEP estimation. In this part, high-resolution GSR mapping products (0.5 m) were overlaid with district polygons, building footprints, and an LULC map to examine multi-scale spatial patterns of rooftop SEP. The third part focuses on the analysis of energy, economic and carbon benefits. In this study, energy-saving potentials, financial viability, profitability, affordability, and lifecycle carbon benefits for rooftop PV systems were estimated (Supplementary Fig. 1). The data sources are summarized in Supplementary Table 4.

Clear-sky GSR model

The clear-sky GSR, defined by the total amount of incoming solar radiation received by a surface under cloud-free conditions, was computed using Eq. (1)[29]. The Solar Analyst tool (Raster Solar Radiation) with the hemispherical viewshed algorithm[40] in ArcGIS Pro 3.4 has been utilized for GSR estimation, considering the roof elevation, orientation, roof gradient, and shadow cast by adjacent taller objects, using digital surface models (DSMs) as a data source.

$$GSR_{modeled,clear} = GSR_{Direct} + GSR_{Diffuse}, \quad (1)$$

where $GSR_{modeled,clear}$ is the clear-sky GSR (kWh/m^2); GSR_{Direct} is the direct solar radiation (kWh/m^2); $GSR_{Diffuse}$ is the diffused solar radiation from the sky (kWh/m^2).

Ångström–Prescott (A–P) GSR model

The A–P regression algorithm, first introduced by Ångström in 1924[27] and modified by Prescott in 1940[28], is widely utilized to calibrate the estimated clear-sky GSR with ground-based GSR and sunshine duration[29,30].

The GSR_{Clear}, calculated using Eq. (1), provides a theoretical estimate under ideal atmospheric conditions, assuming no cloud cover effect. This estimate serves as a critical input for the A–P model to derive the empirical A–P parameters in Eq. (2) through linear regression, establishing a relationship between the theoretical and observed GSR in real-world conditions.

The A–P model was established by two steps. The first step was to derive the optimal A–P parameters with linear regression using Eq. (2).

$$\frac{GSR_{measured,all-sky,KP}}{GSR_{modeled,clear,KP}} = \beta\left(\frac{D_{measured,all-sky,KP}}{D_{modeled,clear,KP}}\right) + \alpha, \quad (2)$$

where $GSR_{measured,all-sky,KP}$ is the measured all-sky GSR at King's Park (kWh/m^2); $GSR_{modeled,clear,KP}$ is the modeled clear-sky GSR at King's Park (kWh/m^2); $D_{measured,all-sky,KP}$ is the measured bright sunshine duration at King's Park under all-sky condition (hours); $D_{modeled,clear,KP}$ is the modeled sunshine duration at King's Park under clear-sky condition (hours); α and β are the A–P parameters to be derived using linear regression techniques.

The second step was to employ the derived A–P parameters to generate a raster layer of predicted all-sky GSR (0.5 m resolution), using Eq. (3).

$$GSR_{pred,all-sky,HK} = GSR_{modeled,clear,HK}\left(\alpha + \beta\frac{D_{measured,all-sky,KP}}{D_{modeled,clear,HK}}\right), \quad (3)$$

where $GSR_{pred,all-sky,HK}$ is the predicted GSR for the entire Hong Kong area under all-sky condition (kWh/m^2); $GSR_{modeled,clear,HK}$ is the modeled GSR for the entire Hong Kong area under clear-sky condition (kWh/m^2); $D_{measured,all-sky,KP}$ is the measured bright sunshine duration under all-sky condition at King's Park (hours); $D_{modeled,clear,HK}$ is the modeled sunshine duration for the entire Hong Kong area under clear-sky condition (hours).

Himawari 8/9 cloud optical thickness derived GSR model

The Himawari 8/9 Cloud Optical Thickness (HCOT)-derived GSR model was established using the random forest regression technique with the Shapley Additive Explanation (SHAP) framework[41]. The modeling process can be divided into three stages, including pre-processing, training, and prediction.

Pre-processing. Raw datasets were converted to GeoTIFF, reprojected to the local coordinate reference system, and clear-sky values set to 0. The daily COT for the entire Hong Kong area was computed using Eq. (4).

$$COT_{i,j} = \sum_{k=1}^{72} COT_{i,j,k}, \tag{4}$$

where $COT_{i,j}$ is the cloud optical thickness value for *ith* year (i = 2016, 2017, …, 2024) and *jth* Julian day (j = 1, 2, …, 365 for non-leap year; j = 1, 2, …, 366 for leap year); $COT_{i,j,k}$ is the cloud optical thickness value for *ith* year, *jth* Julian day, and *kth* observations on *jth* Julian day (k = 1, 2, …, 72). As the HCOT product was derived from cloud radiance, data collection for the HCOT product was restricted to 06:00–18:00 UTC to ensure the validity of cloud detection.

Training. The SHAP framework[41] was incorporated when training the machine learning model using scikit-learn 1.6.1 library in Python[42]. In this stage, daily clear-sky GSR derived from Eq. (1) and daily COT derived from Eq. (4) have been utilized as model inputs, while daily ground observed GSR is used for model training. Additionally, random forest and extreme gradient boosting (XGBoost) are tested and compared. While the XGBoost model is more computationally efficient, we choose the random forest model for its higher accuracy. The detailed training parameters used for developing the random forest model have been listed in Supplementary Table 5. Using Eq. (5), we have developed a random forest regression model for GSR prediction.

$$GSR_{measured,all-sky,i,j} = f\left(GSR_{modeled,clear,i,j}, COT_{i,j}\right), \tag{5}$$

where $GSR_{measured,all-sky,i,j}$ is the measured daily GSR (kWh) at a ground station (King's Park) for *ith* year and *jth* Julian day under all-sky conditions; $GSR_{modeled,clear,i,j}$ is the modeled daily clear-sky GSR (kWh) at King's Park for *ith* year and *jth* Julian day, derived from Eq. (1); $COT_{i,j}$ is the daily cloud optical thickness at King's Park for *ith* year and *jth* Julian day. f is the implicit function for the random forest regression model trained by inputting $GSR_{measured,all-sky,i,j}$, $GSR_{modeled,clear,i,j}$ and $COT_{i,j}$.

Prediction. First, each daily COT image was divided into 2829 tiles with a tile size of 2000 for batch-by-batch processing. Second, the daily COT product was resampled from 5 km to 0.5 m using bilinear interpolation to align with the high-resolution clear-sky GSR dataset and to avoid compromising the model's ability to capture shadow-prone areas. Third, the pre-trained random forest model was employed to predict the all-sky GSR for the entire Hong Kong area, inputting $GSR_{modeled,clear,HK,i,j}$ and $COT_{HK,i,j}$, together with Eq. (6).

$$GSR_{pred,all-sky,HK,i,j} = f\left(GSR_{modeled,clear,HK,i,j}, COT_{HK,i,j}\right), \tag{6}$$

where $GSR_{pred,all-sky,HK,i,j}$ is the predicted daily GSR (kWh) for the entire Hong Kong area under all-sky condition (kWh) for *ith* year and *jth* Julian day; $GSR_{modeled,clear,HK,i,j}$ is the modeled daily clear-sky GSR (kWh) within the entire Hong Kong area for *ith* year and *jth* Julian day; $COT_{HK,i,j}$ is the daily cloud optical thickness within the entire Hong Kong area for *ith* year and *jth* Julian day.

Integration of random forest model with SHAP framework

The SHAP framework was first proposed by ref. 41 based on game theory. Due to its strong adaptability to complex models and high interpretability, the SHAP framework has been widely used in decision-making mechanisms for machine learning. It helps evaluate the importance of each input feature on the predicted model output. The feature importance values for the random forest regression model are summarized in Supplementary Fig. 6.

Validation of GSR models

We employed an independent cross-station validation strategy to test the model performance. We use the pre-trained machine learning model, with the model input of modeled clear-sky daily GSR and observed daily COT, to estimate the all-sky daily GSR at Kau Sai Chau (Period: 2016–2024). Then, we pair the estimated all-sky daily GSR with the ground-observed all-sky daily GSR at Kau Sai Chau for accuracy assessment using the following statistical metrics, including the residue (ε), mean bias error, root mean square error, mean absolute bias error (MABE), and the coefficient of determination (R^2). These metrics were computed using Eqs. (7)–(11), respectively. Kau Sai Chau was selected as the validation site owing to the following reasons: first, due to data scarcity, King's Park has been utilized for model training. Only Kau Sai Chau can be reserved for model validation. Second, Kau Sai Chau features rural setting, different from King's Park with urban setting. We can test if the pre-trained machine learning model can be generalized across diverse urban and rural contexts with distinct microclimate, topography, and shading characteristics.

$$\varepsilon = GSR_{all-sky,KSC} - GSR_{observed,KSC}, \tag{7}$$

where $GSR_{all-sky,KSC}$ is the predicted daily GSR under all-sky conditions at Kau Sai Chau (kWh); $GSR_{observed,KSC}$ is the observed daily GSR at Kau Sai Chau (kWh).

$$MBE = \frac{\sum_i^{2024} \varepsilon_i}{n}, \tag{8}$$

$$RMSE = \sqrt{\frac{\sum_i^{2024} {\varepsilon_i}^2}{n}}, \tag{9}$$

$$MABE = \frac{\sum_i^{2024} |\varepsilon_i|}{n}, \tag{10}$$

$$R^2 = 1 - \frac{\sum_{k=1}^{m} \left(GSR_{Observed,KSC,k} - GSR_{all-sky,KSC,k}\right)^2}{\sum_{k=1}^{m} \left(GSR_{Observed,KSC,k} - \overline{GSR_{Observed,KSC}}\right)^2}, \tag{11}$$

where n is the number of datasets; i is the year (i = 2016, 2017, …, 2024); m is the number of datasets for validation; $GSR_{Observed,KSC,k}$ is the observed GSR at the k_{th} observation at Kau Sai Chau (kWh), and k = 1, 2, …, m. $GSR_{all-sky,KSC,k}$ is the predicted GSR under all-sky conditions at the k_{th} observation at Kau Sai Chau (kWh); $\overline{GSR_{Observed,KSC}}$ is the average value of observed GSR at Kau Sai Chau (kWh).

These statistical metrics help evaluate model performance and identify the optimal GSR model for spatial-temporal analysis of rooftop SEP. The validation results have been plotted in Supplementary Fig. 7. As the random forest model performed better in terms of accuracy, it was chosen for rooftop SEP estimation.

Rooftop SEP estimate

Higher GSR increases electricity generation by PV systems, whereas elevated operating temperatures reduce their electrical efficiency[35]. To account for temperature-induced loss in PV efficiency, daily mean air temperature data recorded at 39 ground stations (2016–2024) in Hong Kong were obtained from the Hong Kong Observatory. These point data were interpolated into continuous raster surfaces using Empirical Bayesian Kriging interpolation technique.

The temperature-dependent electrical efficiency of the PV systems was then computed using Eq. (12)[58],

$$\eta = \eta_{ref} \cdot [1 - \beta\left(T_{air} + \frac{(T_{NOCT} - T_{air}) \cdot GSR_{pred,all-sky}}{GSR_{ref}} - T_{Ref}\right)] \quad (12)$$

where η is the temperature-dependent electrical efficiency of the solar PV system; η_{ref} is the referenced electrical efficiency of the solar PV system at a reference temperature of 25 °C, assumed to be 0.15[58,59]; β is the temperature coefficient (°C^{-1}), assumed to be typically 0.0041 °C^{-1} for monocrystalline silicon[58,59]; T_{air} is the daily mean temperature (°C) recorded at 39 ground stations (2016–2024) in Hong Kong; T_{NOCT} is the nominal operating cell temperature of the PV systems under open-circuit condition (°C), preassigned to be 45 °C[60]; $GSR_{pred,all-sky}$ is the predicted GSR in all-sky conditions (kWh/m^2), derived using the pre-trained random forest model; GSR_{ref} is the referenced GSR, assumed to be 9.6 kWh/m^2, computed by multiplying the global solar flux (800 W/m^2) and mean daily sunshine duration (12 h). T_{Ref} is the reference temperature at the global solar flux of 800 W/m^2.

Rooftop SEP was computed using Eq. (13), the daily all-sky GSR raster, and the building footprint shapefile.

$$SEP_{roof} = GSR_{all-sky} \cdot \eta \cdot A \cdot PR, \quad (13)$$

where SEP_{roof} is the estimated value of rooftop SEP (kWh); $GSR_{all-sky}$ is the predicted GSR under all-sky conditions (kWh/m^2), derived from the pre-trained random forest model; η is the temperature-dependent energy efficiency of the solar PV system, estimated using Eq. (12); A is the available rooftop area (m^2). To comply with the statutory requirements, listed in the "Code and References for Correct Installation of Photovoltaic (PV) System"[61], the usable roof area is preassigned to be 50% of building footprint. *PR* is the performance ratio, preassigned to be 0.8[3].

Energy-saving potential

The contribution of rooftop SEP on the energy-saving potentials (ESPs) for coal, natural gas, and nuclear power resources can be quantified using Eqs. (14)–(16).

$$ESP_{coal} = \frac{SEP_{roof,annual} \cdot CF_{coal} \cdot \gamma_{coal}}{E_{coal}}, \quad (14)$$

where ESP_{coal} is the potential annual reduction in coal consumption (tonnes); $SEP_{roof,annual}$ is the estimated value of annual rooftop SEP (kWh); γ_{coal} is the percentage share of coal consumption for power generation, which is 19%[62]; CF_{coal} is the conversion factor from imperial to metric units, which is $0.45359237 \cdot 10^{-3}$ (tonnes/pound); E_{coal} is the amount of energy generated from coal, preassigned as 0.88 (kWh/pound), suggested by U.S. Energy Information Administration[63].

$$ESP_{NG} = \frac{SEP_{roof,annual} \cdot CF_{NG} \cdot \rho \cdot \gamma_{NG}}{E_{NG}}, \quad (15)$$

where ESP_{NG} is the potential annual reduction in natural gas consumption (tonnes); γ_{NG} is the percentage share of natural gas consumption for power generation, which is 49%[62]; CF_{NG} is the conversion factor from imperial to metric units (0.0283168466 m^3/ft^3); ρ is the typical density of natural gas, preassigned as 0.00068 tonnes/pound; E_{NG} is the amount of energy that can be generated from natural gas, preassigned as 0.13 (kWh/ft^3), suggested by the U.S. Energy Information Administration[63].

$$ESP_{Nuclear} = \frac{SEP_{roof,annual} \cdot \gamma_{Nuclear}}{E_{Nuclear}}, \quad (16)$$

where $ESP_{Nuclear}$ is the potential annual reduction in nuclear power resource consumption (tonnes); $\gamma_{Nuclear}$ is the percentage share of nuclear power resource consumption for power generation, which is 32%[62]; $E_{Nuclear}$ is the amount of energy that can be generated from nuclear power resource, preassigned as 24,000,000 (kWh/kg), suggested by European Nuclear Society[64].

Economic potential

The optimal power capacity of the solar PV system for a certain building roof was computed using Eq. (17).

$$P = \max\left(\frac{SEP_1}{D_1}, \frac{SEP_2}{D_2}, \ldots, \frac{SEP_n}{D_n}\right), \quad (17)$$

where P is the optimal power capacity of solar PV system for a certain building roof (kW); SEP_n is the rooftop SEP either on the n_{th} day or in the n_{th} month (kWh); D_n is the sunshine duration either on the n_{th} day or in the n_{th} month (hours).

The potential annual revenue (HK$) earned by feeding rooftop PV output to the grid under the existing FiT scheme[44] was computed using Eq. (18).

$$\begin{aligned}\phi = \{&SEP_{roof,annual} \cdot HK\$4.0\, kWh^{-1}, for\ P \le 10kW\ SEP_{roof,annual} \\ &\cdot HK\$3.0\, kWh^{-1}, for\ 10kW < P \le 200kW\ SEP_{roof,annual} \\ &\cdot HK\$2.5\, kWh^{-1}, for\ 200kW < P \le 1MW\}\end{aligned} \quad (18)$$

where ϕ is the potential annual revenue of earned from rooftop PV output (HK$); $SEP_{roof,annual}$ is the annual rooftop SEP (kWh). After FiT expiration, we replace the FiT rate with a mean grid retail price of HK$1.5195/kWh for annual revenue computation[65,66].

To assess the cost competitiveness, the LCOE was computed using Eq. (19).

$$LCOE = \frac{CAPEX + \sum_{t=1}^{25} \frac{OPEX_t}{(1+r)^t}}{\sum_{t=1}^{25} \frac{SEP_1 \cdot (1-D)^{t-1}}{(1+r)^t}}, \quad (19)$$

where *CAPEX* is the capital expenditure (HK$). Two scenarios were considered for *CAPEX*, corresponding to the lower (HK$30,000/kW) and higher (HK$50,000/kW) installation cost[20]; t is the typical lifespan of a solar PV system, assumed to be 25 years[43]; $OPEX_t$ is the operational expenditure in the t-th year (HK$). It includes annual operational and maintenance costs (assumed to be 1% of *CAPEX*)[67,68], plus a one-time inverter replacement cost rate of HK$1400/kW incurred in the 15th year[69]; SEP_1 is the annual rooftop SEP in the first year (kWh/year); D is the degradation rate of the solar PV system, assumed to be 0.5%[70]; r is the discount rate, assumed to be 5%[71].

To evaluate the financial viability and profitability, the NPV was computed using Eq. (20).

$$NPV = -CAPEX + \sum_{t=1}^{25} \frac{\phi(1-D)^{t-1} - OPEX_t}{(1+r)^t}, \quad (20)$$

To assess the affordability to prospective adopters, the financial payback period was computed using Eq. (21).

$$FPP = \min\left\{ n \left| \sum_{t=1}^{n} \frac{\phi(1-D)^{t-1} - OPEX_t}{(1+r)^t} \ge CAPEX \right. \right\}, \quad (21)$$

where *FPP* is the financial payback period (years); *n* is the number of years after the rooftop PV installation (Years).

Carbon mitigation potential

The net carbon reduction of a PV system (C_{Net}) was estimated by using Eq. (22), based on the framework proposed in our previous study[72].

$$C_{Net} = C_R - \boldsymbol{C_E} = SEP \cdot EF_C \cdot t - (\boldsymbol{C_M}+\boldsymbol{C_T}+\boldsymbol{C_O}+\boldsymbol{C_D}) \quad (22)$$

where C_R is the carbon reduction of solar PV systems during its typical lifespan (kg-CO_2); $\boldsymbol{C_E}$ is the carbon emission of solar PV systems (kg-CO_2); *SEP* is the annual rooftop SEP (kWh/year); EF_C is the carbon emission factor of electricity generation in the local grid, assumed to be 0.39 kg-CO_2/kWh; *t* is the typical lifespan of a solar PV system, assumed to be 25 years[43]; $\boldsymbol{C_M}$, $\boldsymbol{C_T}$, $\boldsymbol{C_O}$, $\boldsymbol{C_D}$ are the carbon emission during manufacturing, transportation, operation, and end-of-life stages respectively, estimated using Eqs. (23)–(26).

$$\boldsymbol{C_M} = EI_M \cdot CF \cdot EF_M \cdot A \quad (23)$$

where $\boldsymbol{C_M}$ is the carbon emission during manufacturing stage (kg-CO_2); EI_M is the energy consumed during the manufacturing process of solar PV[72], assumed to be 822.2595 MJ/m^2. *CF* is the conversion factor to change the unit from MJ to kWh, which is 0.2778. EF_M is the carbon emission factor of electricity generation in China, assumed to be 0.5572 kg-CO_2/kWh[72]; *A* is the available roof area (m^2).

$$\boldsymbol{C_T} = w \cdot A \cdot d \cdot EF_T \quad (24)$$

Where $\boldsymbol{C_T}$ is the carbon emission during transportation stage (kg-CO_2); *w* is the typical weight of solar PV system[72], which is 0.015 tonnes/m^2; *d* is the average port distance for the solar PVs from the ports in Mainland China to Hong Kong, estimated to be 1689 km. EF_T is the carbon emission factor for the sea transport of solar PV system from the ports in Mainland China to Hong Kong, assumed to be 0.3541 kg-CO_2/tonnes-km[72].

$$\boldsymbol{C_O} = 0.1 \cdot \boldsymbol{C_M} \quad (25)$$

where $\boldsymbol{C_O}$ is the carbon emission during operation stage (kg-CO_2), preassigned to as 0.1% of the carbon emission during the manufacturing process[72]. As PV inverters generally have an operational lifespan of approximately 15 years[73], it is typically necessary to replace them once during the lifecycle of the PV modules.

$$\boldsymbol{C_D} = EI_D \cdot CF \cdot EF_M \cdot A + P \cdot C_{recycle} \quad (26)$$

where $\boldsymbol{C_D}$ is the carbon emission during decommission stage (kg-CO_2); EI_D is the energy consumed during the decommission process of solar PV[72], assumed to be 262.5 MJ/m^2; *P* is the optimal power capacity of solar PV system for a certain building roof (kW), obtained from Eq. (17); $C_{recycle}$ is the carbon emission per unit of power during decommission, which is −129 kg-CO_2/kWp for mono-crystalline solar cells[72].

The carbon payback period (CPBP) was estimated using Eq. (27) following our previous study[72], which evaluates the time required for the rooftop PVs to begin yielding carbon mitigation benefits.

$$CPBP = \frac{C_E}{SEP \cdot EF_C} \quad (27)$$

Uncertainty analysis

We quantified uncertainties in SEP and associated economic metrics (LCOE, NPV, and financial payback period) using an ensemble of 40,000 Monte Carlo simulations at a 90% confidence level[67]. For annual SEP estimates, we randomly and uniformly varied the key model inputs: all-sky GSR estimates (± 1%), utilization factor on unoccupied roof area (70–100%)[74], performance ratio (0.7–0.9)[75], and PV electrical efficiency (± 5%)[3,4,34,58]. This produced a relative uncertainty of ±6.83% for annual SEP.

For the economic metrics, we considered two capex scenarios: lower-capex scenario (HK$30,000/kW) and higher-capex scenario (HK$50,000/kW). In each scenario, we randomly and uniformly varied the following parameters: PV degradation rate (0.2–0.5%)[43], discount rate (5–7.5%)[70], PV lifespan (25–30 years)[71], and the annual SEP estimates (± 6.83%). The resulting relative uncertainties were ±11.79, ±18.92, and ±2.98% for LCOE, NPV, and financial payback period, respectively, under the lower-capex scenario, and ±11.87, ±29.67, and ±8.15% under the higher-capex scenario.

Data availability

The high-resolution (0.5 m) GSR datasets and source data underlying the main figures are available from Figshare at https://doi.org/10.6084/m9.figshare.33349182[76]. The building footprints and administrative district boundaries are available at https://portal.csdi.gov.hk/csdi-webpage/. The LiDAR-derived DSMs are available at https://sdportal.cedd.gov.hk/#/en. The Himawari-8/9 COT datasets are available from JAXA at https://www.eorc.jaxa.jp/ptree/userguide.html. The ground-observed GSR, air temperature and bright sunshine duration datasets are available from the Hong Kong Observatory at https://www.hko.gov.hk/en/index.html. The building-level energy consumption data for commercial buildings in Hong Kong is available from EMSD at https://www.emsd.gov.hk/beeo/en/register/search_eaf.php.

Code availability

The script used to apply the pre-trained machine learning model for all-sky daily GSR estimation is publicly available at https://github.com/Jimmy-Tong/Rooftop_SEP_HK/. The repository contains sample datasets and code to reproduce the model output for testing.

Received: 23 February 2026; Accepted: 8 September 2026;
Published online: 03 October 2026

References

1. Zhang, Z. et al. Worldwide rooftop photovoltaic electricity generation may mitigate global warming. *Nat. Clim. Chang.* **15**, 393–402 (2025).
2. Yang, R. et al. Urban rooftops for food and energy in China. *Nat. Cities* **1**, 741–750 (2024).
3. Zhang, Z. et al. Carbon mitigation potential afforded by rooftop photovoltaic in China. *Nat. Commun.* **14**, 2347 (2023).
4. Joshi, S. et al. High resolution global spatiotemporal assessment of rooftop solar photovoltaics potential for renewable electricity generation. *Nat. Commun.* **12**, 5738 (2021).
5. Forrester, S. P., Montañés, C. C., O'Shaughnessy, E. & Barbose, G. Modeling the potential effects of rooftop solar on household energy burden in the United States. *Nat. Commun.* **15**, 4676 (2024).
6. Jiang, H. et al. Globally interconnected solar-wind system addresses future electricity demands. *Nat. Commun.* **16**, 1–16 (2025).
7. Kammen, D. M. & Sunter, D. A. City-integrated renewable energy for urban sustainability. *Science* **352**, 922–928 (2016).
8. Chen, L. et al. Impacts of photovoltaics and integrated green roofs on urban climate: experimental insights for urban land surface modelling. *Renew. Sustain. Energy Rev.* **217**, 115709 (2025).
9. Electrical and Mechanical Services Department. *Hong Kong Energy End-use Data 2025*. https://www.emsd.gov.hk/filemanager/en/content_762/HKEEUD2025.pdf (Hong Kong SAR Government, 2025).
10. Zhu, R. et al. The effect of urban morphology on the solar capacity of three-dimensional cities. *Renew. Energy* **153**, 1111–1126 (2020).
11. Zhu, R., You, L., Santi, P., Wong, M. S. & Ratti, C. Solar accessibility in developing cities: a case study in Kowloon East, Hong Kong. *Sustain. Cities Soc.* **51**, 101738 (2019).
12. Mohajeri, N. et al. A city-scale roof shape classification using machine learning for solar energy applications. *Renew. Energy* **121**, 81–93 (2018).

13. Bamisile, O., Acen, C., Cai, D., Huang, Q. & Staffell, I. The environmental factors affecting solar photovoltaic output. *Renew. Sustain. Energy Rev.* **208**, 115073 (2025).
14. Li, X., Mauzerall, D. L. & Bergin, M. H. Global reduction of solar power generation efficiency due to aerosols and panel soiling. *Nat. Sustain.* **3**, 720–727 (2020).
15. Sweerts, B. et al. Estimation of losses in solar energy production from air pollution in China since 1960 using surface radiation data. *Nat. Energy* **4**, 657–663 (2019).
16. Wu, S., Chen, B., An, J., Lin, C. & Gong, P. The interplay of cloud cover and 3D urban structures reduces human access to sunlight. *Nat. Cities* **1**, 686–694 (2024).
17. Zhang, X., Shen, L. & Chan, S. Y. The diffusion of solar energy use in HK: what are the barriers? *Energy Policy* **41**, 241–249 (2012).
18. Mah, D. N. Y. et al. Barriers and policy enablers for solar photovoltaics (PV) in cities: perspectives of potential adopters in Hong Kong. *Renew. Sustain. Energy Rev.* **92**, 921–936 (2018).
19. Lo, K. et al. Barriers to adopting solar photovoltaic systems in Hong Kong. *Energy Environ.* **29**, 649–663 (2018).
20. Li, D. H., Cheung, K. L., Lam, T. N. & Chan, W. W. A study of grid-connected photovoltaic (PV) system in Hong Kong. *Appl. Energy* **90**, 122–127 (2012).
21. Dato, P., Durmaz, T. & Pommeret, A. Feed-in tariff policy in Hong Kong: is it efficient? *City Environ. Interact.* **10**, 100056 (2021).
22. Shi, M., Lu, X. & Craig, M. T. Unveiling deployable rooftop solar potential across Chinese cities. *Nat. Cities* **2**, 650–661 (2025).
23. O'Shaughnessy, E., Barbose, G., Wiser, R., Forrester, S. & Darghouth, N. The impact of policies and business models on income equity in rooftop solar adoption. *Nat. Energy* **6**, 84–91 (2021).
24. Shi, M. et al. Technical to deployable potential of rooftop solar photovoltaics. *Nat. Rev. Clean. Technol.* **80**, 1–20 (2026).
25. Wong, M. S. et al. Estimation of Hong Kong's solar energy potential using GIS and remote sensing technologies. *Renew. Energy* **99**, 325–335 (2016).
26. Xu, F., Wong, M. S., Zhu, R. & Dang, Y. Solar cities: multiple-reflection within urban canyons. *ISPRS J. Photogramm. Remote Sens.* **227**, 205–218 (2025).
27. Angstrom, A. Solar and terrestrial radiation. Report to the International Commission for Solar Research on actinometric investigations of solar and atmospheric radiation. *Q. J. R. Meteorol. Soc.* **50**, 121–126 (1924).
28. Prescott, J. A. Evaporation from a water surface in relation to solar radiation. *Trans. R. Soc. South Aust.* **46**, 114–118 (1940).
29. Chen, Z., Yang, B., Zhu, R. & Dong, Z. City-scale solar PV potential estimation on 3D buildings using multi-source RS data: a case study in Wuhan, China. *Appl. Energy* **359**, 122720 (2024).
30. Paulescu, M. et al. Ångström–Prescott equation: physical basis, empirical models and sensitivity analysis. *Renew. Sustain. Energy Rev.* **62**, 495–506 (2016).
31. Liao, X. et al. Fast and accurate estimation of solar irradiation on building rooftops in Hong Kong: a machine learning-based parameterization approach. *Renew. Energy* **216**, 119034 (2023).
32. Xu, L. et al. Hourly solar irradiance estimation and building-surface solar potential assessment via remote sensing and machine learning for data-scarce mountainous regions. *Energy Rep.* **15**, 109017 (2026).
33. Sander, L., Jung, C., Matzarakis, A. & Schindler, D. Global assessment of availability, reliability, and spatiotemporal variability in ground-based solar radiation measurements. *Sol. Energy* **309**, 114458 (2026).
34. Ren, H., Ma, Z., Chan, A. B. & Sun, Y. Optimal planning of municipal-scale distributed rooftop photovoltaic systems with maximized solar energy generation under constraints in high-density cities. *Energy* **263**, 125686 (2023).
35. Poulek, V., Matuška, T., Libra, M., Kachalouski, E. & Sedláček, J. Influence of increased temperature on energy production of roof integrated PV panels. *Energy Build.* **166**, 418–425 (2018).
36. Yan, J., Yang, Y., Elia Campana, P. & He, J. City-level analysis of subsidy-free solar photovoltaic electricity price, profits and grid parity in China. *Nat. Energy* **4**, 709–717 (2019).
37. Lu, L. & Yang, H. X. Environmental payback time analysis of a roof-mounted building-integrated photovoltaic (BIPV) system in Hong Kong. *Appl. Energy* **87**, 3625–3631 (2010).
38. Peng, J. & Lu, L. Investigation on the development potential of rooftop PV system in Hong Kong and its environmental benefits. *Renew. Sustain. Energy Rev.* **27**, 149–162 (2013).
39. Environment and Ecology Bureau. *Hong Kong's Climate Action Plan 2050* https://cnsd.gov.hk/wp-content/uploads/pdf/CAP2050_booklet_en.pdf (Hong Kong SAR Government, 2021).
40. Rich, P., Dubayah, R., Hetrick, W. & Saving, S. Using viewshed models to calculate intercepted solar radiation: applications in ecology. In *1994 ASPRS/ACSM Annual Convention & Exposition: ASPRS Technical Papers* Vol. 1, 524–529 (American Society for Photogrammetry and Remote Sensing, 1994).
41. Lundberg, S. M. & Lee, S. I. A unified approach to interpreting model predictions. *Adv. Neural Inf. Process. Syst.* **30**, 4765–4774 (2017).
42. Pedregosa, F. et al. Scikit-learn: machine learning in Python. *J. Mach. Learn. Res.* **12**, 2825–2830 (2011).
43. Ali, A., Malik, S. A., Shafiullah, M., Malik, M. Z. & Zahir, M. H. Policies and regulations for solar photovoltaic end-of-life waste management: insights from China and the USA. *Chemosphere* **340**, 139840 (2023).
44. Electrical and Mechanical Services Department. *Feed-in Tariff (FiT) - Introduction*. https://re.emsd.gov.hk/english/fit/int/fit_int.html (Hong Kong SAR Government, 2025).
45. Census and Statistics Department. *Table 950-92054: Greenhouse Gas Emissions and Carbon Intensity*. https://www.censtatd.gov.hk/en/web_table.html?id=950-92054# (Hong Kong SAR Government, 2026).
46. Yang, J., Yi, B., Wang, S., Liu, Y. & Li, Y. Diverse cloud and aerosol impacts on solar photovoltaic potential in southern China and northern India. *Sci. Rep.* **12**, 19671 (2022).
47. Song, R. et al. Coal plants persist as a large barrier to the global solar energy transition. *Nat Sustain.* https://doi.org/10.1038/s41893-026-01836-5 (2026).
48. Yin, K. et al. Substantial reduction of solar photovoltaic potential in China by an extreme dust event. *Commun. Earth Environ.* **7**, 44 (2026).
49. Staffell, I., Pfenninger, S. & Johnson, N. A global model of hourly space heating and cooling demand at multiple spatial scales. *Nat. Energy* **8**, 1328–1344 (2023).
50. Chen, W., Hong, J., Yuan, X. & Liu, J. Environmental impact assessment of monocrystalline silicon solar photovoltaic cell production: a case study in China. *J. Clean. Prod.* **112**, 1025–1032 (2016).
51. Wang, M., Mao, X., Gao, Y. & He, F. Potential of carbon emission reduction and financial feasibility of urban rooftop photovoltaic power generation in Beijing. *J. Clean. Prod.* **203**, 1119–1131 (2018).
52. McCormick, P. G. & Suehrcke, H. The effect of intermittent solar radiation on the performance of PV systems. *Sol. Energy* **171**, 667–674 (2018).
53. Alam, M. J. E., Muttaqi, K. M. & Sutanto, D. A novel approach for ramp-rate control of solar PV using energy storage to mitigate output fluctuations caused by cloud passing. *IEEE Trans. Energy Convers.* **29**, 507–518 (2014).
54. Wu, Y. & Zhong, L. Decarbonizing urban residential communities with green hydrogen systems. *Nat. Cities* **2**, 81–92 (2025).
55. Zhang, X., Shen, L., Tam, V. W. & Lee, W. W. Y. Barriers to implement extensive green roof systems: a Hong Kong study. *Renew. Sustain. Energy Rev.* **16**, 314–319 (2012).
56. Building Department. *Code of Practice for Dead and Imposed Loads (2011 Edition)*. https://www.bd.gov.hk/doc/en/resources/codes-

and-references/code-and-design-manuals/DIL2011e.pdf (Hong Kong SAR Government, 2021).
57. Building Department. *Code of Practice for Fire Safety in Buildings 2011 (2024 Edition)*. https://www.bd.gov.hk/doc/en/resources/codes-and-references/code-and-design-manuals/fs_code2011.pdf (Hong Kong SAR Government, 2024).
58. Dubey, S., Sarvaiya, J. N. & Seshadri, B. Temperature dependent photovoltaic (PV) efficiency and its effect on PV production in the world–a review. *Energy Procedia* **33**, 311–321 (2013).
59. Evans, D. L. & Florschuetz, L. W. Cost studies on terrestrial photovoltaic power systems with sunlight concentration. *Sol. Energy* **19**, 255–262 (1977).
60. Hi-MO X6 Scientist. *LR5-54HTH 445~455 M*. https://static.longi.com/L_Gi_LE_PM_T_PMD_059_F131_LR_5_54_HTH_445_455_M_30_30_and_15_Frame_Scientist_V19_9e6db880ac.pdf (Longi, 2023).
61. Building Department, The Government of the Hong Kong Administrative Region. *Code and Reference Correct Installation of Photovoltaic (PV) System*. https://www.bd.gov.hk/en/resources/codes-and-references/pv-panel/index.html (2025).
62. CLP Power Hong Kong Limited. Transition to net zero. In *2023 Sustainability Report*. https://sustainability.clpgroup.com/en/2023/our-sustainability-agenda/transition-to-net-zero (2023).
63. U.S. Energy Information Administration. *How Much Coal, Natural Gas, or Petroleum is Used to Generate a Kilowatt-Hour of Electricity?* https://www.eia.gov/tools/faqs/faq.php?id=667&t=6 (2022).
64. European Nuclear Society. *Fuel Comparison*. https://www.euronuclear.org/glossary/fuel-comparison/ (2025).
65. CLP Power Hong Kong Limited. *CLP Power Reduces 2026 Tariff by 2.6%: Boosting the Economy and Promoting Decarbonisation with HK $270 Million Package*. https://www.clp.com.hk/content/dam/clp-group/channels/media/document/2025/20251118_en.pdf (Press Release, 2025).
66. HK Electric. *HK Electric Announces 2.2% Tariff Reduction for 2026*. https://www.hkelectric.com/documents/en/MediaResources/PressReleases/Documents/20251118_pre_TR%202026_final_website.pdf (Press Release, 2025).
67. Wang, Y. et al. Accelerating the energy transition towards photovoltaic and wind in China. *Nature* **619**, 761–767 (2023).
68. Baldi, D., Moner-Girona, M., Fumagalli, E. & Fahl, F. Planning sustainable electricity solutions for refugee settlements in sub-Saharan Africa. *Nat. Energy* **7**, 369–379 (2022).
69. Peng, J., Yang, H., & Wang, M. *Actual Performances of PV Panels in the Local Environment* https://re.emsd.gov.hk/files/Actual_Performances_of_PV_Panels_in_the_Local_Environment.pdf (Renewable Energy Research Group, Department of Building Services Engineering, The Hong Kong Polytechnic University, 2020).
70. Peters, I. M., Hauch, J., Brabec, C. & Sinha, P. The value of stability in photovoltaics. *Joule* **5**, 3137–3153 (2021).
71. International Renewable Energy Agency (IRENA). *Renewable Power Generation Costs in 2019* https://www.irena.org/-/media/Files/IRENA/Agency/Publication/2020/Jun/IRENA_Power_Generation_Costs_2019.pdf (International Renewable Energy Agency, Abu Dhabi, 2020).
72. Zhu, R. et al. Multi-sourced data modelling of spatially heterogenous life-cycle carbon mitigation from installed rooftop photovoltaics: a case study in Singapore. *Appl. Energy* **362**, 122957 (2024).
73. Woodhouse, M. et al. *On the Path to Sunshot-the Role of Advancements in Solar Photovoltaic Efficiency, Reliability, and Costs (No. NREL/TP--6A20-65872)* (EERE Publication and Product Library, 2016).
74. Electrical and Mechanical Services Department. *Study report of photovoltaic (PV) applications and PV potential on building rooftops in Hong Kong*. https://re.emsd.gov.hk/english/files/2019_Executive_Summary_for_PV_Study_EN.pdf (2019).
75. Liang, H. & You, F. Reshoring silicon photovoltaics manufacturing contributes to decarbonization and climate change mitigation. *Nat. Commun.* **14**, 1274 (2023).
76. Tong, L. Y. et al. Datasets for "Rooftop solar supports carbon-neutral transition in Hong Kong's building sector. *figshare. Dataset*. 10.6084/m9.figshare.33349182 (2026).

Acknowledgements

The authors would like to thank the Japan Aerospace Exploration Agency (JAXA) for providing the Himawari 8/9 datasets that support this study.

Author contributions

Lai Yiu Tong and Zhiwei Li conceptualized and designed the study. Lai Yiu Tong collected and processed the data. Lai Yiu Tong and Zhiwei Li conducted the results analysis and prepared the initial manuscript draft. Lai Yiu Tong, Zhiwei Li, Cheolhee Yoo, Siqi Jia, Rui Zhu, and Jungho Im contributed to the review and editing of the manuscript. All authors approved the manuscript for submission.

Funding

This study was supported by the Fundamental Research Funds for the Central Universities (No. 2042026fg0051) and the National Natural Science Foundation of China (No. 42101357).

Competing interests

The authors declare no competing interests.

Additional information

Supplementary information The online version contains supplementary material available at https://doi.org/10.1038/s44458-026-00157-0.

Correspondence and requests for materials should be addressed to Zhiwei Li or Jungho Im.

Peer review information *Communications Sustainability* thanks the anonymous, reviewer(s) for their contribution to the peer review of this work. Primary Handling Editors: Nandita Basu. A peer review file is available.

Reprints and permissions information is available at http://www.nature.com/reprints

Publisher's note Springer Nature remains neutral with regard to jurisdictional claims in published maps and institutional affiliations.

Open Access This article is licensed under a Creative Commons Attribution-NonCommercial-NoDerivatives 4.0 International License, which permits any non-commercial use, sharing, distribution and reproduction in any medium or format, as long as you give appropriate credit to the original author(s) and the source, provide a link to the Creative Commons licence, and indicate if you modified the licensed material. You do not have permission under this licence to share adapted material derived from this article or parts of it. The images or other third party material in this article are included in the article's Creative Commons licence, unless indicated otherwise in a credit line to the material. If material is not included in the article's Creative Commons licence and your intended use is not permitted by statutory regulation or exceeds the permitted use, you will need to obtain permission directly from the copyright holder. To view a copy of this licence, visit http://creativecommons.org/licenses/by-nc-nd/4.0/.

© The Author(s) 2026